Effects of a Cylindrical Metallic Cavity on the Radiation of Longitudinally Polarized Limited-Diffractive Bessel Beams

Santi C. Pavone, *Senior Member, IEEE*, Loreto Di Donato, *Member, IEEE*, and Gino Sorbello, *Member, IEEE*

***Abstract*—This letter deals with the problem of evaluating the effect of a cylindrical metallic cavity on the radiation of a planar longitudinally polarized Bessel beam launcher, as it could arise in applications related to microwave heating or plasma ignition. A full analytical model is developed to extract fundamental physics insight of the problem at hand. Full-wave numerical simulations by COMSOL multiphysics are used to validate the proposed model, showing fair agreement between simulations and theoretical predictions.**

***Index Terms*—Bessel beam, Green's function, metallic cavity, near-field, radiation.**

I. Introduction

In SOME engineering applications, such as near-field focusing [1], [2], [3], [4], [5], [6], near-field communications [7], wireless power transfer [8], ground-penetrating radars [9], optical micromanipulation [10], [11], and imaging [12], [13], [14], [15], beam diffraction has to be minimized in such a way to not to lose energy and also to focus it in specific spatial regions. Nondiffractive waves, i.e., a family of solutions of Helmholtz equation that does not undergo diffraction when propagating in free-space, have been introduced and investigated in the last decade [16], [17], [18]. Among them, Bessel beams are interesting both from the historical and technical viewpoints. Indeed, since their early introduction by Durnin in 1987 [19], [20] in the optical regime, they have been profitably adopted to radiate well collimated and focused beams in free space [13], [21]. Pure Bessel beams cannot be radiated in free space, since they would require infinite energy or, equivalently, infinite radiating apertures. In this sense, they can be considered as a nonphysical solution, such as plane waves. However, limited-diffractive beams, i.e., Bessel beams focused up to a finite distance called nondiffractive range (NDR), can be instead effectively radiated by finite apertures and carry finite energy. This latter does not constitute a limitation in real-life applications, since the appropriate choice of both aperture size and imposed radial wavenumber on it allows predicting the achievable NDR and, in turn, designing launchers to satisfy application-oriented specific requirements.

Interestingly, in the last decade, high-efficiency Bessel beams have been successfully designed at microwaves and millimeter waves [2], [22], by exploiting different but complementary approaches, such as holography on radial-line slot arrays [4], [6], [9], metasurfaces [23], or leaky-wave-based approaches [3]. Moreover, mature planar technologies, such as printed circuit board (PCB), are available for compact Bessel-beam launcher fabrication so that real applications of Bessel beams at microwaves and millimeter waves do not represent only an idealization, but instead a promising reality.

Bessel beams launchers have been studied mainly for radiation in free space, but they can also find applications when radiating in confined environments, such as cavities. Indeed, the presence of a strong axial (i.e., longitudinal) electric field component, as happens in longitudinally polarized Bessel beams [4], would allow accelerating charged particles [24], [25]. Similarly, the spatially distributed field obtained by multiple Bessel beam reflections inside metallic cavities paves the way to the use of such structures for microwave heating. Moreover, the compression of plasmas inside metallic cylindrical cavities together with their interaction with RF and microwave fields, with RF and microwave fields, allows exciting them in plasma ignition systems [26], [27], [28]. Thus, the presence of metallic cavities needs to be accurately modeled. Indeed, a closed metallic cavity introduces a numerable (i.e., discrete) set of modes for field expansion that perturbs Bessel beam radiation and needs to be accurately considered through the appropriate Green's function. As a limit case, if cavity dimensions are really large in terms of wavelength ($b \to +\infty$), the discrete set of supported modes tends to be almost continuous (thus, resembling free-space continuous spectrum); hence, the beam reconstructed inside the cavity resembles the Bessel beam radiated in free space, as expected.

Due to the inherent azimuthal invariance of impressed magnetic current distribution that radiates a *longitudinally polarized* Bessel beam [4], in this letter we focus on the radiation in circular-symmetric perfect electric conductors (PEC) cavities by considering both analytical modeling and full-wave simulations for validation. Physics insight and relevant wave phenomena connected to beam radiation in bounded domains are then highlighted.

The rest of this letter is organized as follows. In Section II, the analytical formulation of the radiation in a cylindrical metallic cavity of a magnetic current distribution, appropriately shaped to radiate a longitudinally polarized Bessel beam in free space,

Manuscript received 19 October 2022; revised 8 November 2022; accepted 8 November 2022. Date of publication 14 November 2022; date of current version 3 March 2023. The work of Santi C. Pavone was supported by the Department of Electrical, Electronics and Computer Engineering, University of Catania, through PIACERI project (Linea 2D–2E). *(Corresponding author: Santi C. Pavone.)*

The authors are with the Department of Electrical, Electronics, and Computer Engineering (DIEEI), University of Catania, 95123 Catania, Italy, and also with the Istituto Nazionale di Fisica Nucleare (INFN), Laboratori Nazionali del Sud (LNS), 95123 Catania, Italy (e-mail: santi.pavone@unict.it; loreto.didonato@unict.it; gino.sorbello@unict.it).

Digital Object Identifier 10.1109/LAWP.2022.3221889

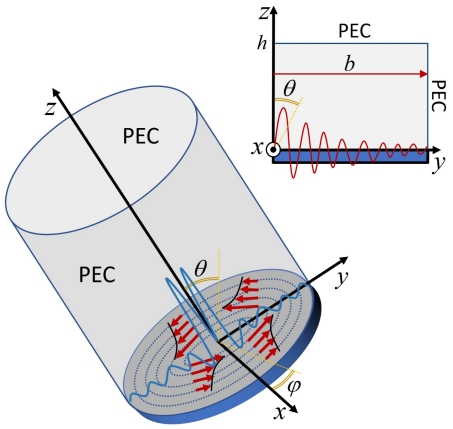

Fig. 1. Geometry of the problem. An azimuthally invariant magnetic current distribution shaped as a first-order Bessel function, able to radiate a longitudinally polarized Bessel beam in free space, radiates inside a cylindrical metallic cavity, thus exciting a perturbed field distribution inside it.

is presented. Then, in Section III, the model is compared with full-wave simulations by COMSOL Multiphysics for validation. Finally, Section IV concludes this letter.

II. Problem Formulation

The geometry of the problem is depicted in Fig. 1. By assuming and suppressing throughout this letter the usual time-harmonic convention $e^{j\omega_0 t}$, being ω_0 the operating angular frequency, a finite azimuthally invariant magnetic current distribution of the form

$$\mathbf{M}(\rho) = M_0 J_1(k_{\rho a}\rho)\Pi\left(\frac{\rho}{2b}\right)\hat{\boldsymbol{\phi}} \tag{1}$$

is impressed at $z = 0$ and radiates inside a cylindrical metallic cavity of radius b and height h. In (1), $\Pi(\cdot)$ is the circular constant function ($\Pi(x/x_0) = 1$ if $|x| \leq x_0/2, \Pi(x/x_0) = 0$ elsewhere), M_0 is the magnetic current complex amplitude, $k_{\rho a} = k\sin\theta_a$ the imposed radial wavenumber, k the free-space wavenumber at the operating frequency, and θ_a the so-called *axicon angle*. For the sake of simplicity, cavity walls are assumed to be made of PEC. As shown in detail in [4], the current distribution in (1) is able to radiate a longitudinally polarized Bessel beam in free space, i.e., a Bessel beam whose electric field z-component is shaped as a zeroth-order Bessel function.

The objective of this letter is to analyze how the radiated beam is perturbed by the presence of a cylindrical metallic cavity, since in general the electromagnetic (EM) field inside it can be written as a superposition of a numerable infinite set of modes, hence the spectrum of the eigenvalues associated to Laplacian operator is discrete. According to Marcuvitz–Schwinger formalism, the EM field by impressed current distributions (either electric, $\mathbf{J}$, or magnetic, $\mathbf{M}$) can be decomposed in its transverse $(\mathbf{E}_t, \mathbf{H}_t)$ and longitudinal (E_z, H_z) components with respect to a prescribed direction. For the problem at hand, it is convenient to use the z-axis. Hence, the transverse EM field components can be written as superposition of transverse electric (TE_z) and magnetic (TM_z) modes [29], namely

$$\mathbf{E}_t(\mathbf{r}) = \sum_{m,n} V_{mn}^{\mathrm{TM}}\mathbf{e}_{mn}^{\mathrm{TM}}(\boldsymbol{\rho}) + \sum_{m,n} V_{mn}^{\mathrm{TE}}\mathbf{e}_{mn}^{\mathrm{TE}}(\boldsymbol{\rho}) \tag{2}$$

$$\mathbf{H}_t(\mathbf{r}) = \sum_{m,n} I_{mn}^{\mathrm{TM}}\mathbf{h}_{mn}^{\mathrm{TM}}(\boldsymbol{\rho}) + \sum_{m,n} I_{mn}^{\mathrm{TE}}\mathbf{h}_{mn}^{\mathrm{TE}}(\boldsymbol{\rho}) \tag{3}$$

in which $\mathbf{e}_{mn}^{\mathrm{TM,TE}}$ ($\mathbf{h}_{mn}^{\mathrm{TM,TE}}$) are the TE/TM electric (magnetic) vector mode functions, whereas $V_{mn}^{\mathrm{TM,TE}}$ ($I_{mn}^{\mathrm{TM,TE}}$) refer to complex modal amplitudes, to be suitably determined. Due to ϕ-invariance and azimuthal polarization of the impressed magnetic current distribution (1), the EM field inside the cavity can be represented only in terms of TM modes, so that $V_{mn}^{\mathrm{TE}} = I_{mn}^{\mathrm{TE}} = 0$. Moreover, the radiated EM field expansion in (2) and (3) can be reduced to a single n-dependent series. Hence, for the problem at hand the transverse field expressions reduce to

$$\mathbf{E}_t(\mathbf{r}) = \sum_n V_{0n}^{\mathrm{TM}}\mathbf{e}_{0n}^{\mathrm{TM}}(\boldsymbol{\rho}), \quad \mathbf{H}_t(\mathbf{r}) = \sum_n I_{0n}^{\mathrm{TM}}\mathbf{h}_{0n}^{\mathrm{TM}}(\boldsymbol{\rho}). \tag{4}$$

The longitudinal EM field component can be calculated by the differentiation of (4) as

$$E_z(\mathbf{r}) = (j\omega\epsilon)^{-1}[\nabla_t \cdot (\mathbf{H}_t \times \hat{\mathbf{z}}) - J_z] \tag{5}$$

$$H_z(\mathbf{r}) = (j\omega\mu)^{-1}[\nabla_t \cdot (\hat{\mathbf{z}} \times \mathbf{E}_t) - M_z] \tag{6}$$

being J_z (M_z) the z-component of electric (magnetic) current that in the following will be assumed to vanish, since (1) represents a purely transverse current distribution. TM_z vector mode functions can be written as the transverse gradient of a normalized set of scalar mode functions ψ_{mn}^{TM}, namely

$$\mathbf{e}_{mn}^{\mathrm{TM}}(\boldsymbol{\rho}) = -\frac{\nabla_t\psi_{mn}^{\mathrm{TM}}(\boldsymbol{\rho})}{k_{t,mn}^{\mathrm{TM}}}, \qquad \mathbf{h}_{mn}^{\mathrm{TM}}(\boldsymbol{\rho}) = \hat{\mathbf{z}} \times \mathbf{e}_{mn}^{\mathrm{TM}}(\boldsymbol{\rho}) \tag{7}$$

being $k_{t,mn}^{\mathrm{TM}}$ the transverse wavenumber associated with TM modes. For the special case of circular cylindrical cavity cross section, bounded by a PEC wall [29], ψ_{mn}^{TM} can be expanded in terms of mth-order Bessel functions; hence, vector mode functions (7) become

$$\mathbf{e}_{mn}^{\mathrm{TM}}(\boldsymbol{\rho}) = -\frac{\exp(-jm\phi)}{b\sqrt{\pi}k_{t,mn}^{\mathrm{TM}}J_{m+1}(k_{t,mn}^{\mathrm{TM}}b)} \cdot \left[\frac{m\sqrt{2}}{\rho}J_m(k_{t,mn}^{\mathrm{TM}}\rho)\hat{\mathbf{p}} - k_{t,mn}^{\mathrm{TM}}J_{m+1}(k_{t,mn}^{\mathrm{TM}}\rho)\hat{\boldsymbol{\rho}}\right] \tag{8}$$

$$\mathbf{h}_{mn}^{\mathrm{TM}}(\boldsymbol{\rho}) = -\frac{\exp(-jm\phi)}{b\sqrt{\pi}k_{t,mn}^{\mathrm{TM}}J_{m+1}(k_{t,mn}^{\mathrm{TM}}b)} \cdot \left[j\frac{m\sqrt{2}}{\rho}J_m(k_{t,mn}^{\mathrm{TM}}\rho)\hat{\mathbf{p}} - k_{t,mn}^{\mathrm{TM}}J_{m+1}(k_{t,mn}^{\mathrm{TM}}\rho)\hat{\boldsymbol{\phi}}\right] \tag{9}$$

in which $\hat{\mathbf{p}} = \left(\hat{\boldsymbol{\rho}} - j\hat{\boldsymbol{\phi}}\right)/\sqrt{2}$ and $k_{t,mn}^{\mathrm{TM}} = \chi_{mn}/b$, being χ_{mn} the zeros of mth-order Bessel functions, and $n \in \mathbb{N}_0$.

To calculate the z-dependence of the forced EM field inside the cavity expressed by (1), an equivalent multimodal transmission-line approach is exploited [29], according to which modal voltage generators v_{mn}^{TM}, whose amplitude can be calculated by projecting the transverse magnetic current distribution on the set of magnetic vector mode functions, namely

$$v_{mn}^{\mathrm{TM}} \equiv v_{0n}^{\mathrm{TM}} = \iint_S \mathbf{M}(\boldsymbol{\rho}) \cdot \mathbf{h}_{mn}^{*}(\boldsymbol{\rho})dS = \frac{2\sqrt{\pi}M_0}{J_1(k_{t,0n}^{\mathrm{TM}}b)} \cdot \frac{k_{t,0n}^{\mathrm{TM}}J_1(k_{\rho a}b)J_0(k_{t,0n}^{\mathrm{TM}}b) - k_{\rho a}J_0(k_{\rho a}b)J_1(k_{t,0n}^{\mathrm{TM}}b)}{k_{\rho a}^2 - (k_{t,0n}^{\mathrm{TM}})^2} \tag{10}$$

being S the cross-sectional surface, are placed at the section $z' = 0$ of z-oriented transmission lines, terminated on a short circuit at $z = h$.

By calculating (10), only modal voltage coefficients of order $m = 0$ contribute (i.e., do not vanish) to EM field expansion (2) and (3); thus, the double series used for field expansion can be simply replaced by a single n-dependent series. For this reason, in the following, the replacement $mn \to 0n$ will be adopted to take into account the previous consideration. By using (10), the modal voltages V_{0n}^{TM} and currents I_{0n}^{TM} are then calculated at each generic section z as

$$V_{0n}^{\mathrm{TM}} = \frac{2\sqrt{\pi}M_0}{J_1(k_{t,0n}^{\mathrm{TM}}b)}\Big[\cos(k_{z,0n}^{\mathrm{TM}}z) - \cot(k_{z,0n}^{\mathrm{TM}}h)\sin(k_{z,0n}^{\mathrm{TM}}z)\Big]\cdot \cdot \frac{k_{t,0n}^{\mathrm{TM}}J_1(k_{\rho a}b)J_0(k_{t,0n}^{\mathrm{TM}}b) - k_{\rho a}J_0(k_{\rho a}b)J_1(k_{t,0n}^{\mathrm{TM}}b)}{k_{\rho a}^2 - (k_{t,0n}^{\mathrm{TM}})^2}$$

$$I_{0n}^{\mathrm{TM}} = \frac{2j\sqrt{\pi}M_0}{J_1(k_{t,0n}^{\mathrm{TM}}b)}\Big[\sin(k_{z,0n}^{\mathrm{TM}}z) + \cot(k_{z,0n}^{\mathrm{TM}}h)\cos(k_{z,0n}^{\mathrm{TM}}z)\Big]\cdot \cdot \frac{k_{t,mn}^{\mathrm{TM}}J_1(k_{\rho a}b)J_0(k_{t,mn}^{\mathrm{TM}}b) - k_{\rho a}J_0(k_{\rho a}b)J_1(k_{t,mn}^{\mathrm{TM}}b)}{k_{\rho a}^2 - (k_{t,mn}^{\mathrm{TM}})^2}$$

being $k_{z,0n}^{\mathrm{TM}} = -j\sqrt{(k_{t,0n}^{\mathrm{TM}})^2 - k^2}$ the longitudinal modal wavenumbers, whose branch cut is chosen in such a way to guarantee the damping of nonpropagating modes (i.e., evanescent) away from the source region (i.e., at $z' = 0$). Finally, by substituting the previous expressions for modal voltages and currents in (2) and (3), the transverse EM field excited inside the cavity by the current distribution given by (1) is

$$\mathbf{E}_t(\mathbf{r}) = -\frac{2M_0}{b}\hat{\boldsymbol{\rho}}\sum_n \Bigg\{ \frac{J_1(k_{t,0n}^{\mathrm{TM}}\rho)}{J_1^2(k_{t,0n}^{\mathrm{TM}}b)}\cdot \cdot \Big[\cos(k_{z,0n}^{\mathrm{TM}}z) - \cot(k_{z,0n}^{\mathrm{TM}}h)\sin(k_{z,0n}^{\mathrm{TM}}z)\Big]\cdot \cdot \frac{k_{t,0n}^{\mathrm{TM}}J_1(k_{\rho a}b)J_0(k_{t,0n}^{\mathrm{TM}}b) - k_{\rho a}J_0(k_{\rho a}b)J_1(k_{t,0n}^{\mathrm{TM}}b)}{k_{\rho a}^2 - (k_{t,0n}^{\mathrm{TM}})^2} \Bigg\} \tag{11}$$

$$\mathbf{H}_t(\mathbf{r}) = \frac{2jM_0}{b}\hat{\boldsymbol{\phi}}\sum_n \Bigg\{ \frac{J_1(k_{t,0n}^{\mathrm{TM}}\rho)}{J_1^2(k_{t,0n}^{\mathrm{TM}}b)}\cdot \cdot \Big[\sin(k_{z,0n}^{\mathrm{TM}}z) + \cot(k_{z,0n}^{\mathrm{TM}}h)\cos(k_{z,0n}^{\mathrm{TM}}z)\Big]\cdot \cdot \frac{k_{t,0n}^{\mathrm{TM}}J_1(k_{\rho a}b)J_0(k_{t,0n}^{\mathrm{TM}}b) - k_{\rho a}J_0(k_{\rho a}b)J_1(k_{t,0n}^{\mathrm{TM}}b)}{k_{\rho a}^2 - (k_{t,0n}^{\mathrm{TM}})^2} \Bigg\}. \tag{12}$$

Similarly, by using (5), the EM field longitudinal component (i.e., z-component) can be calculated as

$$E_z(\mathbf{r}) = -\frac{2M_0}{b\omega\epsilon}\sum_n \Bigg\{ \frac{k_{t,0n}^{\mathrm{TM}}J_0(k_{t,0n}^{\mathrm{TM}}\rho)}{J_1^2(k_{t,0n}^{\mathrm{TM}}b)}\cdot \cdot \Big[\sin\big(k_{z,0n}^{\mathrm{TM}}z\big) - \cot\big(k_{z,0n}^{\mathrm{TM}}h\big)\cos\big(k_{z,0n}^{\mathrm{TM}}z\big)\Big]\cdot \cdot \frac{k_{t,0n}^{\mathrm{TM}}J_1(k_{\rho a}b)J_0\big(k_{t,0n}^{\mathrm{TM}}b\big) - k_{\rho a}J_0(k_{\rho a}b)J_1\big(k_{t,0n}^{\mathrm{TM}}b\big)}{k_{\rho a}^2 - (k_{t,0n}^{\mathrm{TM}})^2} \Bigg\} \tag{13}$$

$$H_z(\mathbf{r}) = 0. \tag{14}$$

The previous equations reveal interesting features of radiated field inside the cavity. Indeed, transverse (longitudinal) field component is shaped as a first (zeroth)-order Bessel function in the radial direction, thus they vanish (exhibit a maximum) on the z-axis. Moreover, the effects of cavity top wall on radiated EM field (i.e., stationary waves due to multiple reflections) are taken into account by the z-dependent term. On the other hand, the contribution of PEC cavity lateral walls to radiated field is instead considered by the b-dependent fraction occurring in (11) and (12) and (13) and (14), which in general diverges when $k_{t,0n} \to k_{\rho a}$.

The theoretical procedure outlined to evaluate (11)–(12) and (13)–(14) allows developing very fast numerical codes for field evaluation in cylindrical (or even more involved) cavities by forced currents known a priori (as happens, for instance, when specific launchers are designed in free space and then placed in closed EM environments), and it is also really helpful for further theoretical generalizations. In Section III, a comparison of the presented analytical model versus full-wave simulations is provided to show the correctness and effectiveness of the approach.

III. Numerical Results and Validation

To validate the theoretical approach discussed in Section II versus a full-wave simulator (COMSOL multiphysics), three examples of cavities are proposed in the following, all fed by the magnetic current distribution (1), with an *axicon angle* [2] of $\theta_a = 15^\circ$, and free-space wavenumber normalized to the wavelength ($k = 2\pi\,\mathrm{rad/m}$). Indeed, as it has been demonstrated in [4] and [6], (1) is able to radiate a longitudinally polarized limited-diffractive Bessel beam in free space. Instead, when it radiates inside a PEC cavity, cavity mode discretization unavoidably occurs, as shown theoretically in (13) and (14) and in (15) and (16). Thus, the Bessel beam radiated in free space is dramatically perturbed by the presence of PEC walls; in particular, stationary patterns due to multiple reflections by PEC lateral and top walls arise, which should be carefully considered in the description of radiated EM field.

To make a fair comparison between the analytical model and full-wave simulations, the relative error

$$\epsilon_{\rho,z} = \frac{|E_{\rho,z}^{\mathrm{an}} - E_{\rho,z}^{\mathrm{sim}}|}{|E_{\rho,z}^{\mathrm{sim}}|} \tag{15}$$

has been introduced, in which $E_{\rho,z}^{\mathrm{an,sim}}$ are the ρ-z electric field components, obtained by the analytical model (apex 'an') or by full-wave simulations (apex 'sim').

In the first one, a PEC cavity of radius $b = 6\lambda$ and height $h = 10\lambda$ is supposed. The normalized electric field z- and ρ-component maps have been calculated by using the analytical model, shown in Fig. 2(a) and (d), and full-wave simulations, as shown in Fig. 2(b) and (c). The relative error (magnitude) between analytical and full-wave field calculations is reported in Fig. 2(c) and (f) for z- and ρ-components, revealing very low values (on average $< 0.5\%$). Hence, both field components are very well reproduced, together with field maxima, minima, and stationary patterns, thus showing a fair reproduction of reflections by lateral and top walls. Thus, the physics of the problem at hand is analytically reproduced by closed-form expressions.

In Fig. 3, a similar approach has been followed by considering an *elongated* cavity of radius $b = 5\lambda$ and height $h = 16\lambda$. Also in this case, a remarkable agreement between analytical and

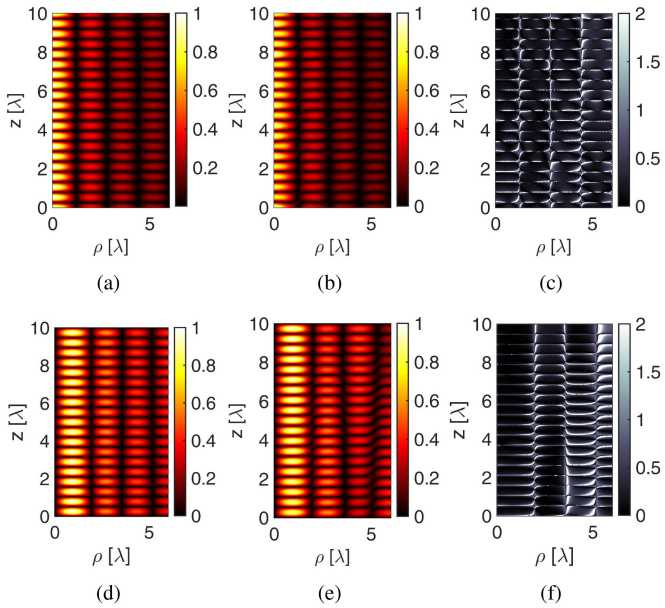

Fig. 2. Field radiated by (1) inside a cavity of radius $b = 6\lambda$ and height $h = 10\lambda$. Normalized electric field z-component calculated by using (a) the analytical model and (b) full-wave simulations. Normalized electric field ρ-component calculated by using (d) the analytical model and (e) full-wave simulations. Relative error between analytical and full-wave field calculation: (c) z-component and (f) ρ-component.

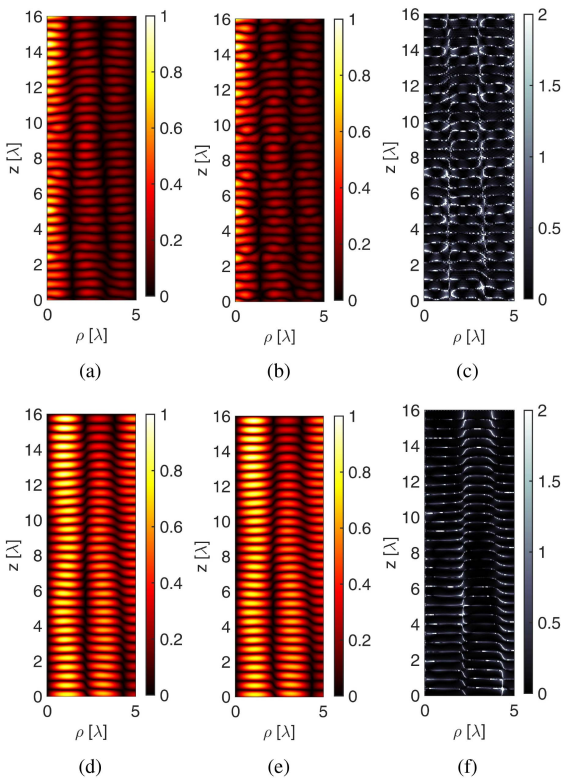

Fig. 3. Field radiated by (1) inside an *elongated* cavity of radius $b = 5\lambda$ and height $h = 15\lambda$. Normalized electric field z-component calculated by using (a) the analytical model and (b) full-wave simulations. Normalized electric field ρ-component calculated by using (d) the analytical model and (e) full-wave simulations. Relative error between analytical and full-wave field calculation: (c) z-component and (f) ρ-component.

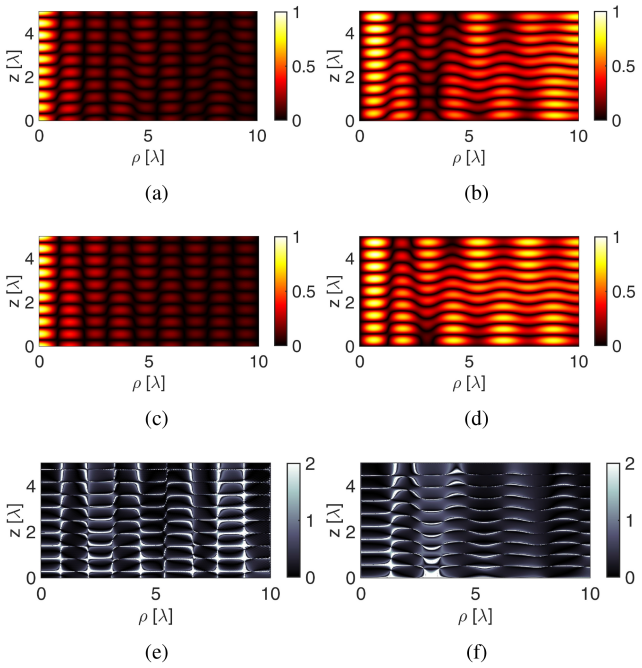

Fig. 4. Field radiated by (1) inside a *short* cavity of radius $b = 10\lambda$ and height $h = 5\lambda$. Normalized electric field z-component calculated by using (a) the analytical model and (c) full-wave simulations. Normalized electric field ρ-component calculated by using (b) the analytical model and (d) full-wave simulations. Relative error between analytical and full-wave field calculation: (e) z-component and (f) ρ-component.

numerical field reconstruction is shown, since the relative error is on average below 0.5%.

Finally, to assess the proposed method also in the case of *short* cavities ($h < b$), an example of radius $b = 10\lambda$ and height $h = 5\lambda$ has been presented in Fig. 4. As it can be inferred from color maps in Fig. 4(e) and (f), the relative error in z-ρ electric field component reconstruction is on average of the same order of magnitude of other examples. It is worth noting that, in correspondence of field nulls or minima, the denominator in (15) becomes very close to zero; hence, it seems that the error in field reconstruction in the presence of minima is large; however, it is a fictitious result, inherently associated with the definition of relative error.

The proposed method is really fast, since it is analytic and requires only a summation over a few n orders. As a rule of thumb for summation truncation over n-index, one has to guarantee that $k_{z,0n}^{\mathrm{TM}}$ is real. In the presented examples, $N_{\max} = 20$ guaranteed high accuracy in field reconstruction.

IV. Conclusion

In this letter, the radiation of a longitudinally polarized limited-diffractive Bessel beam inside a cylindrical metallic cavity has been discussed in detail. A full analytical model has been developed to highlight relevant involved wave phenomena. Moreover, a numerical validation of the analytical model by a full-wave simulator has been presented, showing a remarkable agreement between the two methods. The proposed analysis is motivated by forthcoming applications of focused Bessel beams in near-field in bounded metallic domains, such as for microwave heating and plasma ignition.

REFERENCES

[1] M. Ettorre and A. Grbic, "Generation of propagating Bessel beams using leaky-wave modes," *IEEE Trans. Antennas Propag.*, vol. 60, no. 8, pp. 3605–3613, Aug. 2012.

[2] M. Ettorre, S. C. Pavone, M. Casaletti, M. Albani, A. Mazzinghi, and A. Freni, "Near-field focusing by non-diffracting Bessel beams," in *Aperture Antennas for Millimeter and Sub-Millimeter Wave Applications*. Berlin, Germany: Springer, 2018, pp. 243–288.

[3] W. Fuscaldo, G. Valerio, A. Galli, R. Sauleau, A. Grbic, and M. Ettorre, "Higher-order leaky-mode Bessel-beam launcher," *IEEE Trans. Antennas Propag.*, vol. 64, no. 3, pp. 904–913, Mar. 2016.

[4] S. C. Pavone, M. Ettorre, and M. Albani, "Analysis and design of Bessel beam launchers: Longitudinal polarization," *IEEE Trans. Antennas Propag.*, vol. 64, no. 6, pp. 2311–2318, Jun. 2016.

[5] P. Nepa and A. Buffi, "Near-field-focused microwave antennas: Near-field shaping and implementation," *IEEE Antennas Propag. Mag.*, vol. 59, no. 3, pp. 42–53, Jun. 2017.

[6] S. C. Pavone, M. Ettorre, M. Casaletti, and M. Albani, "Analysis and design of Bessel beam launchers: Transverse polarization," *IEEE Trans. Antennas Propag.*, vol. 69, no. 8, pp. 5175–5180, Aug. 2021.

[7] S. Li and J. Wang, "Adaptive free-space optical communications through turbulence using self-healing Bessel beams," *Sci. Rep.*, vol. 7, no. 1, pp. 1–8, 2017.

[8] J. D. Heebl, M. Ettorre, and A. Grbic, "Wireless links in the radiative near field via Bessel beams," *Phys. Rev. Appl.*, vol. 6, no. 3, 2016, Art. no. 0 34018.

[9] A. Mazzinghi et al., "Large depth of field pseudo-Bessel beam generation with a RLSA antenna," *IEEE Trans. Antennas Propag.*, vol. 62, no. 8, pp. 3911–3919, Aug. 2014.

[10] J. Arlt and K. Dholakia, "Generation of high-order Bessel beams by use of an axicon," *Opt. Commun.*, vol. 177, no. 1–6, pp. 297–301, 2000.

[11] D. McGloin and K. Dholakia, "Bessel beams: Diffraction in a new light," *Contemporary Phys.*, vol. 46, no. 1, pp. 15–28, 2005.

[12] J. Lu and J. F. Greenleaf, "Ultrasonic nondiffracting transducer for medical imaging," *IEEE Trans. Ultrason. Ferroelectr. Freq. Control*, vol. 37, no. 5, pp. 438–447, Sep. 1990.

[13] T. A. Planchon et al., "Rapid three-dimensional isotropic imaging of living cells using Bessel beam plane illumination," *Nature Methods*, vol. 8, no. 5, pp. 417–423, 2011.

[14] S. C. Pavone, G. Sorbello, and L. Di Donato, "On the orbital angular momentum incident fields in linearized microwave imaging," *Sensors*, vol. 20, no. 7, 2020, Art. no. 1905.

[15] S. C. Pavone, G. Sorbello, and L. Di Donato, "Improving physical optics approximation through Bessel beam scattering," *IEEE Antennas Wireless Propag. Lett.*, vol. 20, no. 6, pp. 993–997, Jun. 2021.

[16] R. W. Ziolkowski, "Localized wave physics and engineering," *Phys. Rev. A*, vol. 44, no. 6, 1991, Art. no. 3960.

[17] H. E. H.-Figueroa, M. Z.-Rached, and E. Recami, *Localized Waves*. Hoboken, NJ, USA: Wiley, 2008.

[18] H. E. H.-Figueroa, M. Z.-Rached, and E. Recami, *Non-Diffracting Waves*. Hoboken, NJ, USA: Wiley, 2013.

[19] J. Durnin, "Exact solutions for nondiffracting beams. I. The scalar theory," *J. Opt. Soc. Amer. A*, vol. 4, no. 4, pp. 651–654, 1987.

[20] J. Durnin, J. Miceli Jr., and J. Eberly, "Diffraction-free beams," *Phys. Rev. Lett.*, vol. 58, no. 15, 1987, Art. no. 1499.

[21] K.-S. Lee and J. P. Rolland, "Bessel beam spectral-domain high-resolution optical coherence tomography with micro-optic axicon providing extended focusing range," *Opt. Lett.*, vol. 33, no. 15, pp. 1696–1698, 2008.

[22] W. Fuscaldo and S. C. Pavone, "Metrics for localized beams and pulses," *IEEE Trans. Antennas Propag.*, vol. 68, no. 2, pp. 1176–1180, Feb. 2020.

[23] C. Pfeiffer and A. Grbic, "Controlling vector Bessel beams with metasurfaces," *Phys. Rev. Appl.*, vol. 2, no. 4, 2014, Art. no. 0 44012.

[24] B. Hafizi, E. Esarey, and P. Sprangle, "Laser-driven acceleration with Bessel beams," *Phys. Rev. E*, vol. 55, pp. 3539–3545, 1997.

[25] V. H. Mellado, S. Hacyan, and R. Jauregui, "Trapping and acceleration of charged particles in Bessel beams," *Laser Part. Beams*, vol. 24, no. 4, pp. 559–566, 2006.

[26] W. Tan and T. Grotjohn, "Modeling the electromagnetic excitation of a microwave cavity plasma reactor," *J. Vac. Sci. Technol. A*, vol. 12, no. 4, pp. 1216–1220, 1994.

[27] R. Fredericks and J. Asmussen Jr., "High-density resonantly sustained plasma in a variable-length cylindrical cavity," *Appl. Phys. Lett.*, vol. 19, no. 12, pp. 508–510, 1971.

[28] Y. Hasegawa, K. Nakamura, D. Lubomirsky, S. Park, S. Kobayashi, and H. Sugai, "Microwave plasma generation by the fast rotation and slow pulsation of resonant fields in a cylindrical cavity," *Jpn. J. Appl. Phys.*, vol. 56, no. 4, 2017, Art. no. 046203.

[29] L. B. Felsen and N. Marcuvitz, *Radiation and Scattering of Waves*. Hoboken, NJ, USA: Wiley, 1994.

Open Access provided by 'Università degli Studi di Catania' within the CRUI CARE Agreement